Electronic Supplementary Material (ESI) for RSC Advances.

SUPPORTING INFORMATION

Microfluidic alignment and trapping of 1D nanostructures – a simple fabrication route for single-nanowire field effect transistors

A. Gang,[a,b †] N. Haustein,[a § †] L. Baraban,[a] W. Weber,[b,c] T. Mikolajick,[b,c,d] J. Thiele,[a ¶ *] G. Cuniberti[a,b,e *]

a Institute for Materials Science and Max Bergmann Center of Biomaterials, TU Dresden, 01062 Dresden, Germany.

b Center for Advancing Electronics Dresden (CfAED), TU Dresden, 01062 Dresden, Germany.

c NaMLab gGmbH, 01187 Dresden, Germany.

d Chair of Nanoelectronic Materials, TU Dresden, 01187 Dresden, Germany.

e Dresden Center for Computational Materials Science (DCMS), TU Dresden, 01062 Dresden, Germany.

† These authors contributed equally.

§ Current address: BioMed X Innovation Center, 69120 Heidelberg, Germany

¶ Current address: Department of Nanostructured Materials and Leibniz Research Cluster (LRC), Leibniz-Institut für Polymerforschung Dresden e. V., 01069 Dresden, Germany

* Corresponding authors: thiele@ipfdd.de; g.cuniberti@tu-dresden.de.

Content

Abbreviations

1D, one-dimensional; APTES, 3-aminopropyltriethoxysilane; CFD, computational fluid dynamics; CuO NW, copper (II) oxide nanowire; FET, field effect transistor; NW, nanowire; PDMS, polydimethylsiloxane; SEM, scanning electron microscopy; SiNW, silicon nanowire; UVL, UV lithography.

(1) Fabrication of SU-8 2010-based master structures

We prepared the master structures for our microfluidic channels using SU-8 2010 negative photoresist (MicroChem). Table 1 summarizes all processing steps of our protocol.

Table 1: Summary of all processing steps for fabricating SU-8 2010-based master structures.

Substrate preparation	4'' SSP silicon wafer with native oxide (Siegert Wafer) treated with air plasma (Plasma Prep II, SPI supplies) for 2 min and heated to 95 °C for 10 min
Spin coating of photoresist	Two-step coating protocol: 500 rpm at 100 rpm s^{-1} for 10 s and 3000 rpm at 300 rpm s^{-1} for 45 s
Soft-bake	At 95 °C for 3 min
UV-exposure	In MJB4 manual mask aligner (SÜSS MicroTec), 114 mJ cm^{-2} at 365 nm
Post-exposure bake	At 95 °C for 3.5 min
Development	In mr-Dev 600 for 3 min
Rinsing	In isopropanol
Drying	Under a stream of N_2

(2) PDMS-based soft lithography

Using the SU-8 2010-based master structures, we obtained our microfluidic channels via polydimethylsiloxane (PDMS)-based soft lithography.[1] Table 2 summarizes all processing steps of our protocol.

Table 2: Summary of all processing steps for fabricating microfluidic channels via PDMS-based soft lithography.

Pre-polymer mixing	Mixing of PDMS (Sylgard 184, Dow Corning) base and curing agent 10:1 by weight
Degassing	Under vacuum until no more air bubbles are visible
Casting	Pour liquid pre-polymer mixture onto master structure
Curing	At 45°C for at least 6 h
Mold disassembly	Peel cured PDMS cast from master structure
Storage	Store in dry and dust-free conditions with the indented structure facing away from the storage container

(3) Assembly of microfluidic flow set-up

A flow set-up for the alignment and trapping of NWs consists of a receiver substrate (Si wafer with 200 nm thermal oxide, Active Business Company) and a PDMS stamp containing the microchannel structure. Before combining the PDMS stamp and the receiver substrate, we punched two (inlet and outlet) holes into the PDMS stamp, as depicted in Fig. S1a,b. To prevent any distortion of the PDMS and to make sure, that there was no misalignment between trapping sites and mask alignment marks, we placed the stamp gently on the wafer and waited until the adhesion forces of the PDMS brought the stamp fully into contact with the substrate surface.[2] Then, we attached the tubing via extra PDMS pieces.

We drew the NW suspension through the microchannels under a reduced pressure of 100 mbar applied via a syringe pump at the outlet. For handling small sample volumes (1-2 µL), we used an experimental set-up as depicted in Fig. S1a, where the liquid can be drawn into the channels from a sample tube via an inlet tubing. For handling larger sample volumes, (> 5 µL), we punched a bigger inlet hole (3 mm diameter) into the PDMS stamp and pipetted the NW suspension directly into the microchannels (Fig. S1b).

(4) Layout of the channel structure for aligning and trapping NWs

The broad main channel of our fluidic structure for alignment and trapping of NWs successively branched into progressively smaller sub-channels (Fig. S1c). Over four branching stages 32 sub-channels containing the trapping sites were yielded. Based on the intended 6 µm channel width at the trapping sites, we used a generalized Murray's law to obtain the optimum channel widths at the other sections.

Murray's law is a biomimetic design rule, based on the principle of minimum work, derived by Murray in 1926.[3] Barber and Emerson formulated a generalized version of this law, which allows for calculating the optimum width ratio between parent and daughter vessels in microfluidic manifolds of constant channel height.[4] Table 3 summarizes optimized channel widths at different branching stages for our 10 µm-high structure. Enumerations for the branching stages are the same as depicted in Fig. S1c.

Table 3: Summary of optimized channel widths in our 10 µm-high flow structure at different branching stages. Optimization was carried out on basis of a generalized Murray's law.[34] The branching stages are numbered as in Fig. S1c.

Branching stage	Number of branches	Optimized channel width (µm)
4	4	6[#]
3	2	64
2	2	130
1	2	250
In-/outlet	1	446

[#] At this stage, 6 µm channel width is the default value.

In addition to the channel widths, we optimized the lengths of the branches on the inlet side of the trapping sites. In computational fluid dynamics (CFD) simulations (cf. section 5 of this supplementary information), using Comsol Multiphysics® including the CFD module, we determined the hydrodynamic

entrance length for the sub-channels of each branching stage. The hydrodynamic entrance length is the axial distance before the centerline velocity in a channel reaches 99 % of the fully developed flow profile.[5] We added twice the simulated entrance length to the branches on the inlet side of the trapping sites to allow the flow profile to sufficiently stabilize, so that the NWs had a sufficient amount of space to align within the flow. On the outlet side of the trapping sites no additional channel elongation was required.

Furthermore, we included support posts in the channels at the inlet and outlet regions as well as at the branching stages 1 and 2 (see Fig. 1c). The support posts are required for stabilizing the microfluidic channels, because at channel width-to-height ratio of 10 or higher, the ceiling of the channels usually collapses onto the substrate.[1]

(5) *In silico* study of flow behavior

Using Comsol Multiphysics®, we simulated the flow characteristics inside our microfluidic structure to optimize the channel geometries (see section 4 in these supplementary information). A software-built flow chamber was used as a 3D model. A system operating with a uniform, incompressible Newtonian fluid and under the no-slip boundary condition was assumed. Since the NW suspensions that we used were based on the solvent isopropanol, we chose to apply its specific material properties in our models. The walls were assigned to be PDMS or inlet and outlet, respectively. Table 4 summarizes the specific material properties.

Table 4. Material properties used in the COMSOL Multiphysics flow simulation model.

Property name	**Value**
Density of PDMS ρ_{PDMS}	970 kg m^{-3}
Young's modulus E_{PDMS}	$7.5 \cdot 10^5$ Pa
Poisson's ratio v_{PDMS}	0.5
Density of isopropanol $\rho_{isopropanol}$	781 kg m^{-3}
Dynamic viscosity $\mu_{isopropanol}$	0.0025 Pa·s
Pressure at inlet p_{in}	$1 \cdot 10^5$ Pa
Pressure at outlet p_{out}	$0.9 \cdot 10^5$ Pa

In Fig. S1c and Fig. S1d the simulated flow velocities in the utilized flow structure are depicted. It is visible that the velocity reaches its maximum at the trapping sites. In the other sections of the structure the velocity is lower and, more importantly, very uniform. Therefore, we assume that each inflowing NW can end up in any of the trapping sites with equal probability.

(6) Tilt of trapped NWs

In our experiments we observed that the SiNWs are tilted by 21°±5° on average with respect to the inflow channel wall, as depicted in Fig. S1e. The tilt of the NWs was included in the latter electrode design for contacting the NWs.

(7) NW suspension preparation

In our study we used two kinds of NWs:

(i) Monodisperse SiNWs, P-I-P doped, diam. × L 150 nm ± 30 nm × 20 µm ± 2 µm, in isopropanol, $1 \cdot 10^6$ wires mL^{-1} (Sigma Aldrich).

(ii) Polydisperse CuO NWs, grown via oxidation of Cu foil at 500 °C in air for 12 h.[6] NWs were subsequently suspended in isopropanol via sonication.

Since isopropanol as used for suspending the NWs is known to swell PDMS,[7] we mixed the suspensions 1:1 with deionized water before the flow experiments. This dilution of the organic solvent minimized the swelling of PDMS, and no distortions occurred between the trapping sites and the alignment marks.

In case of SiNWs, we usually used suspension volumes below 5 µL, so that for these samples the flow set-up assembly depicted in Fig. S1a was preferred. For CuO NWs, we used suspension volumes of 10 to 20 µL, so that for these samples the flow set-up assembly depicted in Fig. S1b was preferred.

(8) Mask alignment mark deposition

The mask alignment marks were made of 3-aminopropyltriethoxysilane (APTES). The channels for the alignment mark deposition had an opening at the side of the PDMS stamp. Therefore, we brought drops of APTES in contact with the channels, and the silane entered the channels via capillary forces.[8] Inside the channels the APTES molecules bound covalently to the oxide surface and/or cross-linked among each other via their three hydrolyzable groups.[9] After inserting the APTES into the channels, we waited at least 12 h to allow for completion of the cross-linking procedure before dismounting the PDMS stamp from the receiver substrate.

The APTES-based alignment marks have the advantage that they are insoluble in organic solvents, so that they do not vanish when spin coating photoresist onto the substrate as required for the subsequent UV-lithography (UVL) for contacting the wires. However, as ethanol was released during the condensation reaction of APTES, which is also known to swell PDMS,[7] we observed minor deformations of the microchannels during mask alignment mark deposition. These deformations slightly decreased the accuracy of the mask alignment during UVL. Therefore, we are currently also investigating other options to deposit solvent-resistant alignment marks on a receiver substrate.

(9) Contacting of NWs

After dismounting the microfluidic flow set-up, we utilized standard UVL for contacting the trapped NWs. Using APTES-based alignment marks, we defined the contact positions via AZ5214e image reversal photoresist (Micro Chemicals). Table 5 summarizes all steps for processing the resist.

Table 5. Summary of all processing steps for defining the positions of the NW contacts using AZ5214e image reversal photoresist.

Substrate cleaning	- Dismounting of PDMS stamp - Cut-off of wafer parts that were not covered by the PDMS stamp to remove uneven APTES remaining at the edges - Cleaning of substrate in isopropanol (without any sonication) and via plasma treatment (Plasma Prep II, SPI supplies)
Spin coating of photoresist	At 3500 rpm, 4000 rpm s^{-1} for 50 s
Prebake	At 120 °C for 1.5 min
UV-exposure	In MJB4 manual mask aligner (SUSS MicroTec), 38 mJ cm^{-2} at 365 nm
Reversal bake	At 120 °C for 1.5 min
Flood exposure	In MJB4 manual mask aligner (SUSS MicroTec), 570 mJ cm^{-2} at 365 nm
Development	In AZ 726 MIF developer for 1 min
Rinsing	In water
Drying	Under a stream of N_2

For SiNWs, the electrode material was Ni (175 nm, High Resolution Ion Beam Coater, Gatan). Shortly before Ni deposition, we dipped the samples in 1% HF for 40 s to remove the native SiO_2 shell. After metal deposition and lift-off in acetone, we rinsed the samples in isopropanol and dried them under a stream of N_2. Subsequently, we annealed the samples in forming gas (N_2:H_2 10:1, 10 mbar, 450 °C, 3 min, ATV SRO-706 Reflow Oven, ATV Technologies) to lower the contact resistance.

For the CuO NWs, the electrode material was Cr/Au (5 nm/110 nm, UNIVEX 300, Oerlikon Leybold Vaccum). After metal deposition and lift-off in acetone, we rinsed the samples with isopropanol and dried them under a stream of N_2.

(10) Device characterization

For measuring I_{SD}-V_{SD} characteristics of the SiNW devices, we used a PM8 Prober (Cascade Microtech) in combination with a B1505A Power Device Analyzer/Curve Tracer including two High Power Source/Monitor Unit Modules (Agilent Technologies).

For measuring the I_{SD}-V_{SD} characteristics of the CuO NW devices, we used a Keithley Source Meter 2604B in combination with a DPP105-V-AI-S micropositioner (Cascade Microtech) probe station.

In both cases the gate voltage was applied from the back of the substrate wafers.

For scanning electron microscopy investigations, we used an XL 30 ESEM-FEG environmental scanning electron microscope (SEM; Philips).

The statistics in Fig. 2c are based on the data of 8, 13 and 8 FET devices with 0, 1 and 2 contacted SiNWs, respectively.

(11) Supplementary figures

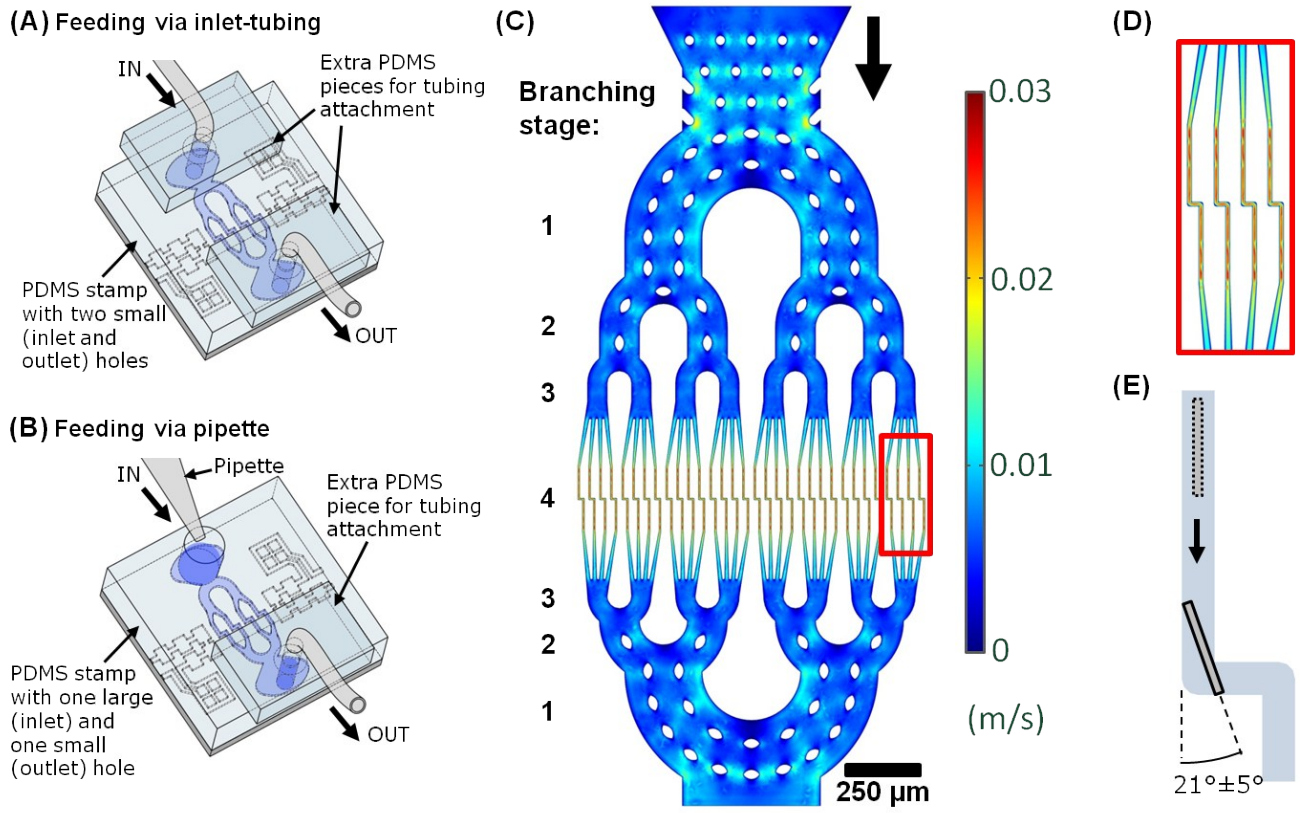

Figure S1. (a), (b) Schematic assembly of microfluidic flow set-ups for trapping NWs from suspension. Suspensions are drawn through channels under reduced pressure of 100 mbar applied via a syringe pump at the outlet channel. Tubing is first attached to extra PDMS pieces which are then bound to the PDMS stamp containing the microchannels. (b) Punching a large inlet hole into the PDMS stamp allows for direct pipetting of NW suspensions into the microchannels. (c) Layout of our microfluidic channel for alignment and trapping of 1D nanostructures, including the numbering of the branching stages and simulated flow velocities. Flow direction indicated by arrow. (d) Enlarged view on red labeled section in Fig. S1c, showing the simulated flow velocities at the trapping sites. (e) Schematic trapping behavior of SiNWs.

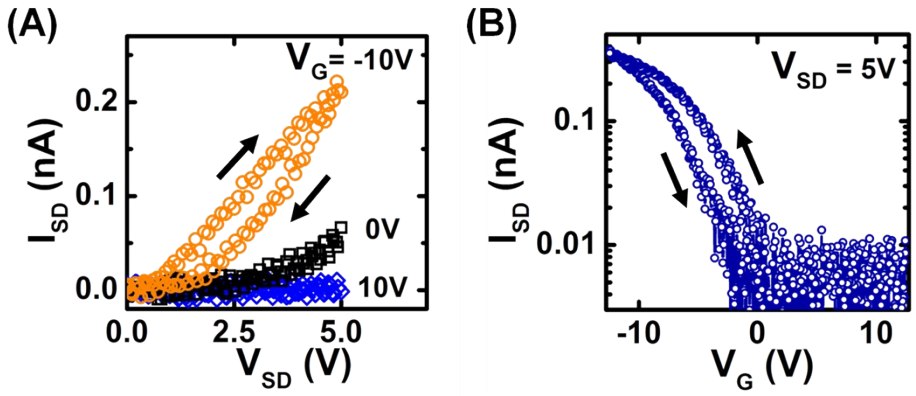

Figure S2. Representative behavior of single-SiNW FETs recorded with the device highlighted in Fig. 2a. (a) I_{SD}-V_{SD} hystereses at different gate voltages: orange circles, black squares, blue diamonds correspond to V_G = 10 V, 0 V, 10 V respectively. (b) I_{SD}-V_G hysteresis recorded at V_{SD} = 5 V.

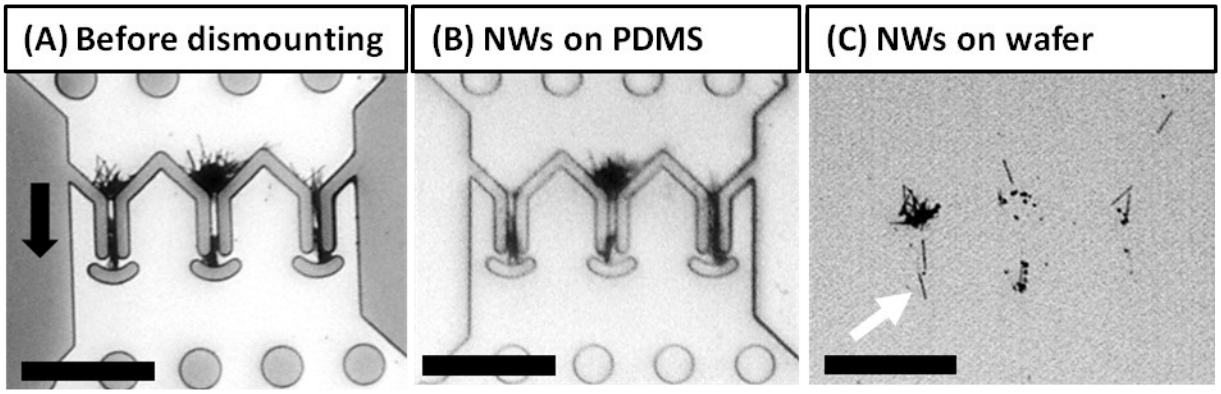

Figure S3. Optical microscopy images of trapping experiment with NW trapping structure utilized in preliminary experiments. The black arrow indicates the flow direction. Scale bars denote 100 µm. Although this trapping structure does not provide sufficient control over the NW positioning, it can be used for trapping large amounts of NWs, for studying the interactions between NWs and PDMS stamp, and NWs and receiver substrate, respectively. (a) Before dismounting the flow assembly, large amounts of NWs are trapped in the intended trapping sites, but also in other sections of the channel. (b) After dismounting the alignment chamber, a large proportion of the trapped NWs adheres to the PDMS stamp, assumingly due to the high adhesion forces of the PDMS.[2] (c) On the wafer, only two non overlapping NWs are left at the trapping site, indicated by the white arrow.

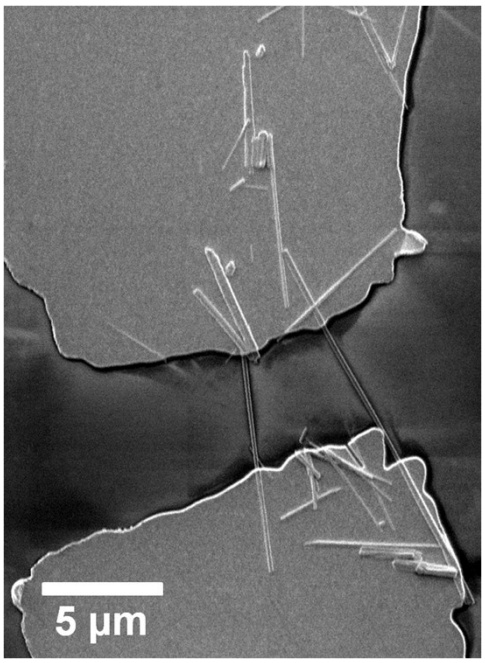

Figure S4. SEM image of a CuO NW FET with two contacted NWs fabricated with our approach. There are many CuO NWs of varying lengths in the vicinity of the FET, indicating polydispersity of the CuO NWs in suspension. The longest NWs in this image are not longer than 15 µm.

References

1 Y. Xia and G. M. Whitesides, *Annu. Rev. Mater. Sci.*, 1998, **28**, 153–184.

2 J. C. McDonald and G. M. Whitesides, *Acc. Chem. Res.*, 2002, **35**, 491–499.

3 C. D. Murray, *Proc. Natl. Acad. Sci. U. S. A.*, 1926, **12**, 207.

4 R. W. Barber and D. R. Emerson, *Microfluid. Nanofluidics*, 2008, **4**, 179–191.

5 R. K. Shah and A. L. London, *Laminar Flow Forced Convection in Ducts: A Source Book for Compact Heat Exchanger Analytical Data*, Academic Press, 2014.

6 X. Jiang, T. Herricks and Y. Xia, *Nano Lett.*, 2002, **2**, 1333–1338.

7 J. N. Lee, C. Park and G. M. Whitesides, *Anal. Chem.*, 2003, **75**, 6544–6554.

8 E. Kim, Y. Xia and G. M. Whitesides, *Nature*, 1995, **376**, 581–584.

9 P. Van Der Voort and E. F. Vansant, *J. Liq. Chromatogr. Relat. Technol.*, 1996, **19**, 2723–2752.